

Helmholtz algebraic solitons

This article has been downloaded from IOPscience. Please scroll down to see the full text article.

2010 J. Phys. A: Math. Theor. 43 085212

(<http://iopscience.iop.org/1751-8121/43/8/085212>)

View [the table of contents for this issue](#), or go to the [journal homepage](#) for more

Download details:

IP Address: 171.66.16.158

The article was downloaded on 03/06/2010 at 08:57

Please note that [terms and conditions apply](#).

Helmholtz algebraic solitons

J M Christian^{1,3}, G S McDonald¹ and P Chamorro-Posada²

¹ Joule Physics Laboratory, School of Computing, Science and Engineering, Materials & Physics Research Centre, University of Salford, Salford M5 4WT, UK

² Departamento de Teoría de la Señal y Comunicaciones e Ingeniería Telemática, Universidad de Valladolid, ETSI Telecomunicación, Campus Miguel Delibes s/n, 47011 Valladolid, Spain

E-mail: j.christian@salford.ac.uk

Received 17 September 2009, in final form 9 December 2009

Published 8 February 2010

Online at stacks.iop.org/JPhysA/43/085212

Abstract

We report, to the best of our knowledge, the first exact analytical algebraic solitons of a generalized cubic–quintic Helmholtz equation. This class of governing equation plays a key role in photonics modelling, allowing a full description of the propagation and interaction of broad scalar beams. New conservation laws are presented, and the recovery of paraxial results is discussed in detail. The stability properties of the new solitons are investigated by combining semi-analytical methods and computer simulations. In particular, new general stability regimes are reported for algebraic bright solitons.

PACS numbers: 42.65.–k, 42.65.Tg, 42.65.Wi, 05.45.Yv

(Some figures in this article are in colour only in the electronic version)

1. Introduction

Solitons are robust, self-localizing waves that can exist in a system when linear spreading effects are opposed by nonlinearity [1]. Their prevalence in mathematical physics is largely due to a relatively small set of universal equations governing a wide range of systems [2]. Solitons tend to be constructed from hyperbolic functions (such as sech and tanh) of the space and/or time coordinates, and are thus exponentially localized wavepackets. However, universal equations can often also support algebraic solitons—particular solutions that are constructed from rational functions. Such solutions are less tightly localized than their hyperbolic counterparts [3]; their tails fall off with a power-law distribution, i.e. *algebraically*.

Perhaps the simplest universal equations with algebraic soliton solutions are of the modified Korteweg–de Vries (KdV) type [4]. KdV-type models, for example, underpin Fermi–Pasta–Ulam descriptions of lattice dynamics [5]. Algebraic solitons are encountered in fluid mechanics as solutions to the Davey–Stewartson [6] and Benjamin–Ono [7] equations. Deep water waves and ion-acoustic waves in plasmas can be described by algebraic solitons of the derivative–nonlinear Schrödinger (NLS) [8] and the Kadomtsev–Petviashvili

³ Author to whom any correspondence should be addressed.

equations [2, 3, 9]. In photonics, algebraic solitons occur in such contexts as Raman scattering [10], self-induced transparency [11] (Maxwell–Bloch-type systems), pulse propagation in dispersive fibres [12] (derivative-NLS), electromagnetic modes of planar waveguides [13] (dual power-law NLS) and solitary-wave polaritons [14] (Boussinesq equation). Coupled modes and periodic systems can also support KdV- and NLS-type algebraic ‘gap solitons’, respectively [15]. Finally, the Klein–Gordon models in ϕ^4 – ϕ^6 theories of particle physics also admit algebraic solutions [16]. This brief summary aims to illustrate that algebraic solitons are fundamental excitations in nonlinear science.

In this paper, we are especially interested in the seminal works by Hayata and Koshiba (who derived the first dual power-law NLS algebraic solitons) [13], and Micallef *et al* (who later showed that these solitons arise mathematically from a particular limit of a hyperbolic solution family) [17]. We report what we believe to be the first algebraic solitons for a nonlinear Helmholtz (NLH) equation. NLH-type models are also universal, appearing whenever the Laplacian is present, e.g. in fluidic, plasma, acoustic and optical nonlinear contexts. Here we consider spatial solitons in uniform two-dimensional planar waveguides, though our general results also have a wider mathematical appeal. A spatial soliton is a stationary beam that can emerge as a dominant electromagnetic mode when diffractive broadening (linear spreading) is exactly balanced by self-lensing (a nonlinear change in the local refractive index of the host medium) [18].

2. Helmholtz soliton theory

2.1. The role of Helmholtz equations

Helmholtz equations play a fundamental role in photonics modelling. They provide a platform for describing *any* experimental arrangement that exploits broad beams in off-axis contexts. It turns out that even the most fundamental ‘building block’ optical geometries have intrinsically angular characters. A pertinent example is the multiplexing of two or more beams at arbitrary angles (with respect to the reference direction) and orientations (with respect to each other). Another example is material interface effects, where beam incidence, transmission and reflection angles at the boundary between dissimilar media may be of arbitrary magnitude.

While paraxial theory well describes the small-angle limit of scalar multiplexing [19] and interface [20] configurations, only recently have their arbitrary-angle properties been explored in detail [21, 22]. These recent analyses relied upon detailed knowledge of the exact analytical soliton solutions to the governing Helmholtz equations. Such models are suitable for addressing the issue of oblique-propagation effects because they respect a fundamental symmetry: in uniform media, there is no distinction between the spatial dimensions. For example, in two-dimensional planar waveguides, the transverse and longitudinal directions are physically equivalent. This spatial symmetry is absent from paraxial theory, and Helmholtz angular corrections to key predictions may exceed 100%.

2.2. Field and envelope equations

In Helmholtz modelling [23, 24], one tends to adopt the scalar approximation whereby the beam waist w_0 is assumed to be much larger than the free-space carrier wavelength λ . Order-of-magnitude corrections to the governing equation, which arise from the polarization-scrambling term $\nabla(\nabla \cdot \mathbf{E})$ in Maxwell’s equations [25–27], are thus unnecessary. Such corrections are routinely based upon a single parameter-of-smallness, $\varepsilon \equiv \lambda/w_0$, and are necessary when $\varepsilon \sim O(1)$. Here, we consider only those contexts where the inequality $\varepsilon \ll O(1)$ is always rigorously satisfied.

For a continuous-wave scalar electric field $\tilde{E}(x, z, t) = E(x, z) \exp(-i\omega t) + \text{c.c.}$ with angular frequency ω , and where $E(x, z)$ satisfies the Maxwell field equation [23, 24], one has

$$\left(\frac{\partial^2}{\partial z^2} + \frac{\partial^2}{\partial x^2} \right) E(x, z) + \frac{\omega^2 n^2}{c^2} E(x, z) = 0. \quad (1)$$

The spatial coordinates, x and z , appear with equal status so that diffraction is fully two dimensional (i.e. occurring in the transverse and longitudinal directions). The refractive index is taken to be $n(|E|) = n_0 + n_{\text{NL}}(|E|)$, where n_0 is the linear index at frequency ω , $n_{\text{NL}}(|E|) = -n_\sigma |E|^\sigma + n_{2\sigma} |E|^{2\sigma}$ is the field-dependent part, n_σ and $n_{2\sigma}$ are small positive constants and the exponent $\sigma > 0$. This classic type of dual power-law distribution appears frequently in photonics; for instance, one might interpret it as an approximation of a quite general model for saturation, namely $n_{\text{NL}}(|E|) = -n_\sigma |E|^\sigma / [1 + (n_{2\sigma}/n_\sigma) |E|^\sigma]$. Various choices of the parameter set ($n_\sigma, n_{2\sigma}, \sigma$) capture Kerr [18, 19], single power-law [28], cubic-quintic [29] and quadratic-cubic [14] nonlinearities. Many authors have studied this model in its most general form [13, 17, 30–32]. With advances in materials science and fabrication, it may one day be possible to tailor dielectric media with arbitrary values of σ for a whole range of information communication and technology applications.

For a weak optical nonlinearity, where $|n_{\text{NL}}(|E|)| \ll n_0$, one has that $n^2(|E|) \simeq n_0^2 + 2n_0 n_{\text{NL}}(|E|)$. To facilitate comparison with paraxial theory, z is chosen to be the longitudinal (reference) direction, and $E(x, z)$ is expressed as $E(x, z) = E_0 u(x, z) \exp(ikz)$. Without further approximation, one can derive the envelope equation:

$$\kappa \frac{\partial^2 u}{\partial \zeta^2} + i \frac{\partial u}{\partial \zeta} + \frac{1}{2} \frac{\partial^2 u}{\partial \xi^2} - \alpha |u|^\sigma u + \gamma |u|^{2\sigma} u = 0. \quad (2)$$

Here, $\zeta = z/L_D$ and $\xi = 2^{1/2}x/w_0$, where $L_D = kw_0^2/2$ is the diffraction length of a reference Gaussian beam, $k = n_0 k_0$ is the wavenumber of the carrier wave and $k_0 = \omega/c = 2\pi/\lambda$. The inverse beam width is quantified by $\kappa \equiv 1/(kw_0)^2 = \varepsilon^2/4\pi^2 n_0^2 \ll O(1)$. Finally, the parameters α and γ are related to the constant E_0 . A convenient normalization that could be adopted is $E_0 \equiv (n_0/n_\sigma L_D k)^{1/\sigma}$, so that $\alpha = 1$ and $\gamma = E_0^\sigma (n_{2\sigma}/n_\sigma)$. For mathematical completeness, however, both α and γ will be retained in the presented solutions. The corresponding paraxial model [13, 17] can be recovered by neglecting the first term in equation (2), which is just the slowly varying envelope approximation (SVEA).

3. Helmholtz bright solitons

The full generality of the ∂_{zz} operator has been preserved in equations (1) and (2). For instance, both models are bidirectional and thus support forward- and backward-propagating fields. It is important to note that forward and backward beams are distinguishable only by their propagation direction with respect to the reference axis. In all other respects, the solutions are physically identical to each other since they are related through a 180° rotation. We now show that equation (2) possesses a variety of exact analytical solutions.

3.1. Hyperbolic solitons

Equation (2) admits two families of exact analytical hyperbolic bright soliton:

$$u(\xi, \zeta) = \eta_h \left[A_h \cosh \left(\sigma \sqrt{2\beta} \frac{\xi + V\zeta}{\sqrt{1 + 2\kappa V^2}} \right) - 1 \right]^{-1/\sigma} \times \exp \left[\pm i \sqrt{\frac{1 + 4\kappa\beta}{1 + 2\kappa V^2}} \left(-V\xi + \frac{\zeta}{2\kappa} \right) \right] \exp \left(-i \frac{\zeta}{2\kappa} \right), \quad (3a)$$

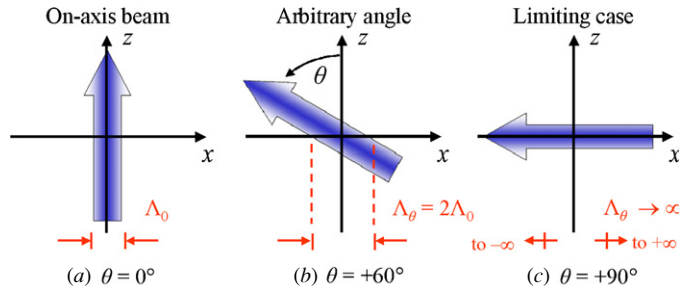


Figure 1. Schematic diagram illustrating the geometry of a forward-propagating Helmholtz soliton. (a) The on-axis beam whose width in the (x, z) frame is $\Lambda_\theta = \Lambda_0$. (b) During oblique propagation at angle θ , the projected beam width is given by $\Lambda_\theta = \Lambda_0 \sec \theta = 2\Lambda_0$ when $|\theta| = 60^\circ$ (to scale). (c) In the extreme case of $|\theta| = 90^\circ$, the beam appears to be infinitely broad when observed from the (x, z) frame.

$$A_h \equiv \left[1 + \frac{(2 + \sigma)^2}{1 + \sigma} \left(\frac{\gamma}{\alpha^2} \right) \beta \right]^{1/2}, \tag{3b}$$

$$\eta_h \equiv \left(\frac{2 + \sigma}{\alpha} \beta \right)^{1/\sigma}. \tag{3c}$$

The beam width measured by an observer in the (x, z) frame is $\Lambda = (1 + 2\kappa V^2)^{1/2} \Lambda_0$, where $\Lambda_0 \equiv (1/\sigma)(2\beta)^{-1/2}$ and V is the conventional transverse velocity parameter. The forward solution (upper sign) describes an exponentially localized beam propagating at an angle $\theta = \tan^{-1}[(2\kappa)^{1/2}V]$ with respect to the $+z$ direction, where $-\infty \leq V \leq +\infty$ corresponds to $-90^\circ \leq \theta \leq +90^\circ$ (this beam is shown schematically in figure 1); the backward solution (lower sign) describes a similar beam evolving in the opposite direction. Solution (3) is characterized by the internal parameter β whose physical significance will shortly become clear.

3.2. Algebraic solitons

Two families of algebraic soliton can be obtained by taking the limit $\beta \rightarrow 0$ in the hyperbolic solutions (3):

$$u(\xi, \zeta) = \eta_a \left[a^2 \left(\frac{\xi + V\zeta}{\sqrt{1 + 2\kappa V^2}} \right)^2 + 1 \right]^{-1/\sigma} \exp \left[\pm i \frac{1}{\sqrt{1 + 2\kappa V^2}} \left(-V\xi + \frac{\zeta}{2\kappa} \right) \right] \exp \left(-i \frac{\zeta}{2\kappa} \right), \tag{4a}$$

$$\eta_a \equiv \left[\left(\frac{2\alpha}{\gamma} \right) \left(\frac{1 + \sigma}{2 + \sigma} \right) \right]^{1/\sigma}, \tag{4b}$$

$$a^2 \equiv \left(\frac{2\alpha^2}{\gamma} \right) \frac{\sigma^2(1 + \sigma)}{(2 + \sigma)^2}. \tag{4c}$$

Solution (4) is determined uniquely for any choice of material parameters (α, γ, σ) ; its amplitude profile is classified as ‘Lorentzian’ when $\sigma = 1$, ‘sub-Lorentzian’ when $\sigma < 1$ and ‘super-Lorentzian’ when $\sigma > 1$. The algebraic bright soliton (4) is weakly localized, with relatively slow power-law asymptotics, $|u(\xi, \zeta)| \sim |\xi + V\zeta|^{-2/\sigma}$ as $|\xi + V\zeta| \rightarrow \infty$. The beam becomes more localized as σ decreases, and such narrowing is off-set by an increase in the

peak amplitude. This relationship follows directly from the nature of a solitary wave: any increase in diffraction must be balanced by an increase in self-focusing.

Theoretical modelling is ultimately concerned with physical phenomena in the laboratory (i.e. the (x, z)) frame. To this end, it is desirable to be able to move easily from scaled to unscaled quantities and coordinates. Such transformations between Helmholtz equations (1) and (2) are fully self-consistent—i.e. exact in their handling of the phase and propagation angle of the beam—since the generality of the (in-plane) Laplacian, $\nabla^2 \equiv \partial_{zz} + \partial_{xx}$, is maintained. In contrast, such transformations can be hindered by the SVEA, where the longitudinal phase shift is always implicitly approximated.

In the (x, z) frame, the longitudinal phase shift $\Delta\phi$ accrued by the hyperbolic soliton (3) during propagation from $z = z_1$ to $z = z_2$ is

$$\Delta\phi = k_0 n_0 \cos\theta (1 + 4\kappa\beta)^{1/2} \Delta z, \tag{5}$$

where $\Delta z \equiv z_2 - z_1$. When $\beta \rightarrow 0$, one has that $\Delta\phi \sim k_0 n_0 \cos\theta \Delta z$, and the phase shift is then identical to that picked up by a plane wave propagating in a purely linear medium with the refractive index n_0 . It is in this sense that algebraic solitons have been interpreted as the threshold for linear wave propagation (i.e. where the carrier wave of the soliton does not ‘see’ the nonlinearity) [17]. The relationship between the algebraic soliton (4) and the linear wave threshold clearly involves the phase in the laboratory reference frame, so an exact transition from hyperbolic to algebraic solutions, valid across the entire range of propagation angles, requires a Helmholtz description.

Analytic continuation of β into the domain $\beta < 0$ can yield delocalized waves whose amplitude profiles are periodic in the transverse direction (since $\cosh(i\Theta) = \cos\Theta$). The forward and backward periodic waves are given by

$$u(\xi, \zeta) = \eta_p \left[A_p \cos \left(\sigma \sqrt{2|\beta|} \frac{\xi + V\zeta}{\sqrt{1 + 2\kappa V^2}} \right) - 1 \right]^{-1/\sigma} \times \exp \left[\pm i \sqrt{\frac{1 - 4\kappa|\beta|}{1 + 2\kappa V^2}} \left(-V\xi + \frac{\zeta}{2\kappa} \right) \right] \exp \left(-i \frac{\zeta}{2\kappa} \right), \tag{6}$$

where $A_p \equiv (1 - |\beta|/|\beta|_{\max})^{1/2}$, $|\beta|_{\max} \equiv (1 + \sigma)(\alpha^2/\gamma)/(2 + \sigma)^2$ and $\eta_p \equiv [-(2 + \sigma)|\beta|/\alpha]^{1/\sigma}$. These solutions exist provided $0 < |\beta| < |\beta|_{\max}$. Propagation (as opposed to evanescence) of the periodic wave requires $|\beta| < 1/4\kappa$. This condition places a physical limit on the smallest transverse period of nonlinear wavetrains in relation to the optical wavelength; such considerations are absent from paraxial theory [17]. In parameter regimes of interest, for example, $\alpha = 1$, $\gamma \leq O(1)$, $\sigma = O(1)$ and $\kappa \ll O(1)$, one finds that the first of these two conditions is nearly always satisfied before the second comes into play (we also note that the second inequality has no analogue in paraxial theory). The connection between hyperbolic, algebraic and periodic waves is illustrated in figure 2.

3.3. Spatial symmetry properties

The symmetry between a forward beam and its backward counterpart can be made explicit by combining the two beams into a single solution. The trigonometric relations $\cos\theta = 1/(1 + 2\kappa V^2)^{1/2}$ and $\sin\theta = (2\kappa)^{1/2} V/(1 + 2\kappa V^2)^{1/2}$ allow one to eliminate V so that the hyperbolic soliton (3) can be written as

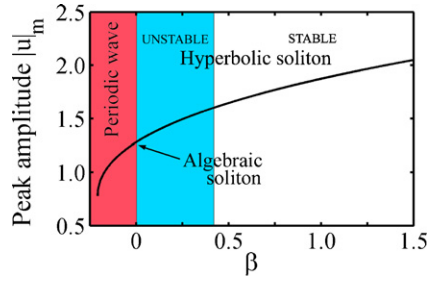


Figure 2. Peak amplitude $|u|_m$ of solution (3) as a function of β for $\sigma = 1.4$ (within the conditionally stable regime, as discussed in section 4). $\beta > 0$ corresponds to hyperbolic soliton (3), and $\beta = 0$ to algebraic soliton (4). The hyperbolic soliton is unstable against small perturbations when $0 < \beta < \beta_{\min} \simeq 0.42$ (blue shaded area). The domain $\beta < 0$ (red shaded area) is accessed through analytic continuation, where one finds a transversely periodic wave. Other parameters: $\alpha = \gamma = 1$.

$$u(\xi, \zeta) = \eta_h \left\{ A_h \cosh \left[\sigma \sqrt{2\beta} \left(\xi \cos \theta + \frac{\zeta}{\sqrt{2\kappa}} \sin \theta \right) \right] - 1 \right\}^{-1/\sigma} \times \exp \left[i \sqrt{\frac{1 + 4\kappa\beta}{2\kappa}} \left(-\xi \sin \theta + \frac{\zeta}{\sqrt{2\kappa}} \cos \theta \right) \right] \exp \left(-i \frac{\zeta}{2\kappa} \right). \quad (7a)$$

In a similar way, the algebraic soliton (4) becomes

$$u(\xi, \zeta) = \eta_a \left[a^2 \left(\xi \cos \theta + \frac{\zeta}{\sqrt{2\kappa}} \sin \theta \right)^2 + 1 \right]^{-1/\sigma} \times \exp \left[i \frac{1}{\sqrt{2\kappa}} \left(-\xi \sin \theta + \frac{\zeta}{\sqrt{2\kappa}} \cos \theta \right) \right] \exp \left(-i \frac{\zeta}{2\kappa} \right). \quad (7b)$$

The propagation angle appearing in solutions (7a) and (7b) now satisfies $-180^\circ \leq \theta \leq +180^\circ$, while the remaining parameters are unchanged. One can also re-express the pair of periodic solutions (6) in this type of symmetric form.

Oblique evolution is a potentially dominant Helmholtz contribution since the beam broadening factor $(1 + 2\kappa V^2)^{1/2} = \sec \theta$ is unbounded: it may be of *any* order *irrespective* of κ and the system nonlinearity. For example, the moderate angle $|\theta| = 60^\circ$ implies that $2\kappa V^2 = 3$, and an observer in the (x, z) frame thus perceives the beam width to have doubled relative to its on-axis value (see figure 3). As $|\theta| \rightarrow 90^\circ$, one has that $2\kappa V^2 \rightarrow \infty$ and the beam appears to be infinitely broad when viewed from the (x, z) frame (where propagation takes place perpendicularly to the reference direction). This geometrical property of Helmholtz solutions appears in the delocalized wave (6) as an increase in the spatial period Γ , where $\Gamma = (1 + 2\kappa V^2)^{1/2} \Gamma_0$ and $\Gamma_0 \equiv 2\pi / [\sigma(2|\beta|)^{1/2}]$. Off-axis effects alone can thus define a scenario in which the angular nonparaxial correction can assume any order $0 < 2\kappa V^2 \leq \infty$ (equivalent to $0 < |\theta| \leq 90^\circ$) while the broad beam inequality $\kappa \simeq \varepsilon^2 \ll O(1)$ is always fully satisfied.

3.4. Conservation laws

Using quite general field-theoretic techniques [33], one can derive three conserved quantities associated with equation (2) that represent the energy-flow, momentum and Hamiltonian, respectively:

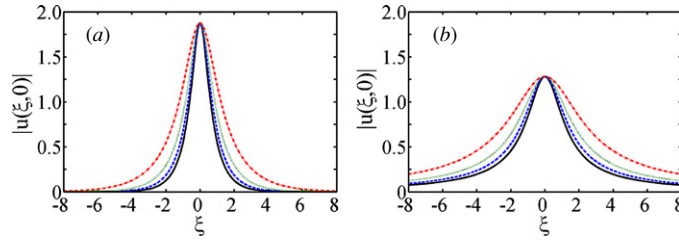


Figure 3. Angular beam broadening effect. (a) Hyperbolic soliton (3) with $\beta = 1$. (b) Algebraic bright soliton (4), obtained in the limit that $\beta \rightarrow 0$. Solid line (black): $\theta = 0^\circ$ (the paraxial profile); dashed line (blue): $|\theta| = 30^\circ$; dotted line (green): $|\theta| = 45^\circ$; dot-dashed line (red): $|\theta| = 60^\circ$ (where the beam width appears to have doubled, relative to its on-axis value). Other parameters: $\sigma = 1.4$ and $\alpha = \gamma = 1$.

$$W = \int_{-\infty}^{+\infty} d\xi \left[|u|^2 - i\kappa \left(u^* \frac{\partial u}{\partial \zeta} - u \frac{\partial u^*}{\partial \zeta} \right) \right], \tag{8a}$$

$$M = \int_{-\infty}^{+\infty} d\xi \left[\frac{i}{2} \left(u^* \frac{\partial u}{\partial \xi} - u \frac{\partial u^*}{\partial \xi} \right) - \kappa \left(\frac{\partial u^*}{\partial \zeta} \frac{\partial u}{\partial \xi} + \frac{\partial u^*}{\partial \xi} \frac{\partial u}{\partial \zeta} \right) \right], \tag{8b}$$

$$H = \int_{-\infty}^{+\infty} d\xi \left[\frac{1}{2} \frac{\partial u^*}{\partial \xi} \frac{\partial u}{\partial \xi} - \kappa \frac{\partial u^*}{\partial \zeta} \frac{\partial u}{\partial \zeta} + \alpha \frac{|u|^{2+\sigma}}{1 + \frac{1}{2}\sigma} - \gamma \frac{|u|^{2(1+\sigma)}}{1 + \sigma} \right]. \tag{8c}$$

By writing solution (3) as $u(\xi, \zeta) = F(s) \exp[i\phi(\xi, \zeta)]$, where F is the (real) amplitude distribution and $s \equiv (\xi + V\zeta)/(1 + 2\kappa V^2)^{1/2}$, the integrals in equations (8a)–(8c) can be expressed more compactly:

$$W = \pm(1 + 4\kappa\beta)^{1/2} P, \tag{9a}$$

$$M = \frac{V}{\sqrt{1 + 2\kappa V^2}} [(1 + 4\kappa\beta)P - 2\kappa Q], \tag{9b}$$

$$H = \frac{W}{2\kappa} - \frac{1}{\sqrt{1 + 2\kappa V^2}} \left(\frac{1}{2\kappa} \right) [(1 + 4\kappa\beta)P - 2\kappa Q]. \tag{9c}$$

The quantities P and Q are given by

$$P \equiv \int_{-\infty}^{+\infty} ds F^2(s) = \frac{2}{\sqrt{2\beta}} \left(\frac{\eta_h^2}{\sigma} \right) \int_0^{+\infty} dy [A_h \cosh(y) - 1]^{-2/\sigma}, \tag{9d}$$

$$Q \equiv \int_{-\infty}^{+\infty} ds \left[\frac{d}{ds} F(s) \right]^2 = 2\sqrt{2\beta} \left(\frac{\eta_h^2 A_h^2}{\sigma} \right) \int_0^{+\infty} dy \sinh^2(y) [A_h \cosh(y) - 1]^{-(2+2/\sigma)}. \tag{9e}$$

The upper (lower) sign in equation (9a) denotes the energy-flow invariant for the forward (backward) beam. By taking the limit $\beta \rightarrow 0$ and substituting for the algebraic soliton (4), it can be shown that

$$P = \sqrt{\pi} \left(\frac{\eta_a^2}{a} \right) \frac{\Gamma(2/\sigma - 1/2)}{\Gamma(2/\sigma)} \tag{10a}$$

and

$$Q = \sqrt{\pi} \left(\frac{2\eta_a^2 a}{\sigma(2 + \sigma)} \right) \frac{\Gamma(2/\sigma + 1/2)}{\Gamma(2/\sigma + 1)}, \tag{10b}$$

where Γ denotes the Gamma function and $0 < \sigma < 4$. Interestingly, Helmholtz bright solitons are also found to satisfy the free-particle relationship $\partial H/\partial M = \partial_V H/\partial_V M = V$, where $\partial_V \equiv \partial/\partial V$. Aside from their physical importance, the integrals in equations (8a)–(8c) allow one to monitor the integrity of the algorithm used to solve equation (2) numerically [34].

3.5. The paraxial limit

The corresponding paraxial model [13, 17] can be obtained from equation (2) by invoking the SVEA, whereby the operator $\kappa \partial_{\zeta\zeta}$ is neglected. It is therefore intuitive that when $\kappa \partial_{\zeta\zeta} \rightarrow 0$, all Helmholtz contributions to beam evolution are negligible, and one should uncover the predictions of paraxial theory. This type of recovery procedure is more subtle than simply setting $\kappa = 0$. Instead, one is obliged to consider a simultaneous multiple limit [35].

To recover the paraxial solution of Micallef *et al* [17] from the hyperbolic soliton (3), one must allow $\kappa \rightarrow 0$ (broad beam), $\kappa\beta \rightarrow 0$ (moderate nonlinear phase shift) and $\kappa V^2 \rightarrow 0$ (negligible propagation angle). We first consider the asymptotic behaviour of the forward solutions, where $\theta \rightarrow 0^\circ$. When applied to the hyperbolic soliton, the triple limit leads to

$$u(\xi, \zeta) \sim \eta_h \{A_h \cosh[\sigma \sqrt{2\beta}(\xi + V\zeta)] - 1\}^{-1/\sigma} \exp \left[-iV\xi + i \left(\beta - \frac{V^2}{2} \right) \zeta \right]. \quad (11a)$$

The β parameter can thus be identified with the on-axis longitudinal phase shift in the corresponding paraxial solution. A similar convergence of the Helmholtz algebraic soliton (4) to its paraxial counterpart requires $\kappa \rightarrow 0$ and $\kappa V^2 \rightarrow 0$, so that

$$u(\xi, \zeta) \sim \eta_a [a^2(\xi + V\zeta)^2 + 1]^{-1/\sigma} \exp \left(-iV\xi - i \frac{V^2}{2} \zeta \right). \quad (11b)$$

By applying the multiple limit to the conserved quantities in equations (9a)–(9c), one obtains the familiar paraxial invariants $W \sim P$, $M \sim VP$ and $H \sim \frac{1}{2}V^2P - \beta P + Q$ for the hyperbolic soliton (the algebraic solution requires $\beta \rightarrow 0$ in the expression for H) [31]. For the backward beams, where $|\theta| \rightarrow 180^\circ$, application of the same multiple limit yields

$$u(\xi, \zeta) \sim \eta_h \{A_h \cosh[\sigma \sqrt{2\beta}(\xi + V\zeta)] - 1\}^{-1/\sigma} \exp \left[iV\xi - i \left(\beta - \frac{V^2}{2} \right) \zeta \right] \exp \left(-i2 \frac{\zeta}{2\kappa} \right) \quad (11c)$$

and

$$u(\xi, \zeta) \sim \eta_a [a^2(\xi + V\zeta)^2 + 1]^{-1/\sigma} \exp \left(iV\xi + i \frac{V^2}{2} \zeta \right) \exp \left(-i2 \frac{\zeta}{2\kappa} \right), \quad (11d)$$

respectively, while the invariants become $W \sim -P$, $M \sim VP$ and $H \sim \frac{1}{2}V^2P - 3\beta P + Q - P/\kappa$. Since the latter set of results retain κ -dependent contributions, it is clear that backward fields have no analogue in paraxial theory. This confirms the fact that paraxial models can support wave propagation in a single longitudinal direction only.

4. Stability of Helmholtz bright solitons

Linear analysis has predicted that plane-wave solutions to NLH equations with arbitrary dispersive nonlinearity functions are modulationally stable in the same parameter regions as their paraxial counterparts [36]. However, the stability of localized solutions against arbitrary perturbations is a much more interesting problem: such stability is a key property of solitons. Without loss of generality, we set $\alpha = \gamma = 1$ throughout this section.

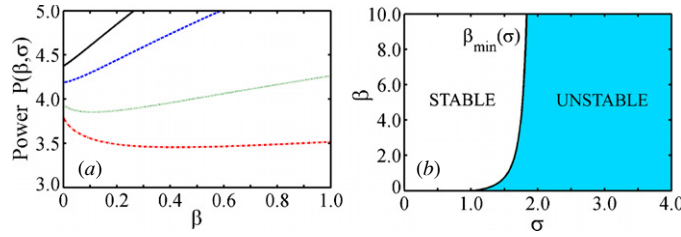


Figure 4. Stability characteristics of hyperbolic solitons. (a) Variation of the beam power P with β (solid line (black): $\sigma = 0.9$; dashed line (blue): $\sigma = 1.0$; dotted line (green): $\sigma = 1.2$; dot-dashed line (red): $\sigma = 1.4$). For $0 < \sigma \leq 1$, the solutions are unconditionally stable ($dP/d\beta > 0$ for all $\beta \geq 0$). For $1 < \sigma < 2$, the solutions are conditionally stable, so that $dP/d\beta > 0$ only when $\beta > \beta_{\min}(\sigma)$. (b) The boundary between stable and unstable solutions in the (σ, β) plane is determined (numerically) by the curve $\beta_{\min}(\sigma)$.

4.1. Analysis

The stability of paraxial bright solitons (11a) has been studied by Micallef *et al* [17] using the well-known Vakhitov–Kolokolov (VK) criterion [30, 37]. Spatial symmetry allows the same criterion to predict the stability properties of Helmholtz solitons [36, 38]. This is because an isolated off-axis beam can always be observed from the ‘on-axis’ frame of reference by means of a rotation of the coordinate axes. In the on-axis frame, where $V = \kappa V^2 = 0$, beams with $\kappa \ll O(1)$ and $\kappa \beta \ll O(1)$ are quasi-paraxial since the forward solution (3) exhibits only an $O(\kappa)$ correction to the longitudinal phase shift.

The VK criterion states that bright solitons can be stable against small perturbations if $dP/d\beta > 0$, where

$$P(\beta; \sigma) \equiv \int_{-\infty}^{+\infty} d\xi |u(\xi, \zeta; \beta; \sigma)|^2 \quad (12)$$

(we note, in passing, that equations (12) and (9d) are formally identical for paraxial solitons). Satisfaction of the VK criterion is a necessary but not sufficient condition for stability [36]; simulations are essential to establish the robustness of solutions against arbitrarily large perturbations. Hyperbolic solitons are predicted to be unconditionally stable when $0 < \sigma \leq 1$ since, for that range of σ , the VK inequality $dP/d\beta > 0$ is satisfied for any $\beta \geq 0$. However, figure 4(a) reveals that when $1 < \sigma < 2$, the slope $dP/d\beta > 0$ only when β exceeds a minimum value, denoted by β_{\min} . Regions of stability in the (σ, β) plane are thus separated by a boundary represented by the curve $\beta_{\min}(\sigma)$ (see figure 4(b)). When $\sigma \geq 2$, the VK criterion predicts that the soliton is always unstable since $dP/d\beta < 0$ for $\beta \geq 0$.

4.2. Hyperbolic solitons

The stability of hyperbolic solitons is considered through the perturbed input beam

$$u(\xi, 0) = \eta_h \left[A_h \cosh(\sigma \sqrt{2\beta} \xi) - 1 \right]^{-1/\sigma} \exp \left(-iV \sqrt{\frac{1 + 4\kappa\beta}{1 + 2\kappa V^2}} \xi \right), \quad (13)$$

whose launching angle is $\theta = \tan^{-1}[(2\kappa)^{1/2}V]$. By applying a rotational transformation [39], one can see that the initial condition (13) is equivalent to an on-axis Helmholtz soliton whose width has been reduced by a factor of $(1 + 2\kappa V^2)^{1/2} = \sec \theta$. For $\kappa = 10^{-3}$ ($\kappa = 10^{-4}$), launching angles of $|\theta| = 10^\circ, 20^\circ, 30^\circ$ and 40° correspond to transverse velocities of

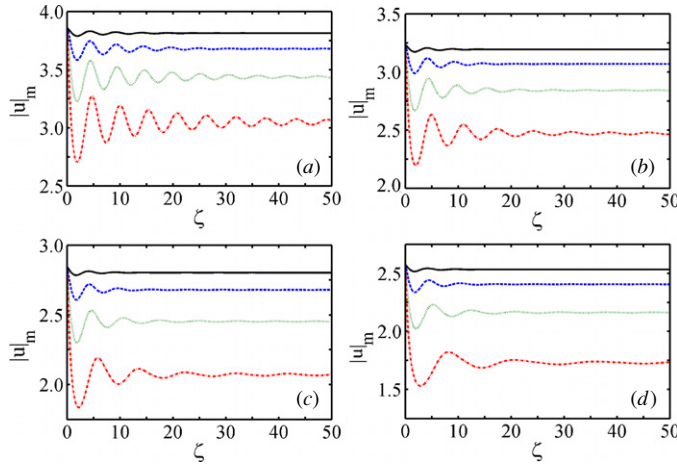


Figure 5. Evolution of the peak amplitude $|u|_m$ of a perturbed hyperbolic soliton with $\beta = 1$ when (a) $\sigma = 0.5$, (b) $\sigma = 0.6$, (c) $\sigma = 0.7$ and (d) $\sigma = 0.8$. Solid lines (black): $|\theta| = 10^\circ$; dashed lines (blue): $|\theta| = 20^\circ$; dotted lines (green): $|\theta| = 30^\circ$; dot-dash lines (red): $|\theta| = 40^\circ$.

$|V| \simeq 3.94, 8.14, 12.91$ and 18.76 ($|V| \simeq 12.47, 25.74, 40.82$ and 59.33), respectively. These angles are clearly non-trivial and lie outside the scope of paraxial theory.

In the unconditionally stable domain ($0 < \sigma \leq 1$), evolution is generally characterized by monotonically decreasing oscillations in the beam parameters (amplitude, width, and area = amplitude \times width). These oscillations are accompanied by a small amount of radiation, and they disappear as $\zeta \rightarrow \infty$ to leave a stationary state (see figure 5). Solitons with $0 < \sigma \leq 1$ can thus generally be interpreted as stable fixed-point attractors: the emission of radiation throughout reshaping provides a mechanism for local dissipation while the system remains globally conservative [36, 38]. As discussed in the preceding subsection, there should be no instability in the range $0 < \sigma \leq 1$ (as prescribed by the VK inequality). However, simulations have revealed that as $\sigma \rightarrow 1$, sufficiently large perturbations can induce a diffractive instability whereby the amplitude of the beam tends to zero as $\zeta \rightarrow \infty$.

To gain insight into the propagation properties of conditionally stable hyperbolic solitons (where $1 < \sigma < 2$), it is instructive to recognize that the power $P_{\text{in}}(\beta, \sigma, V)$ of the perturbed input beam (13) is related to the power $P(\beta, \sigma)$ of the unperturbed beam by

$$P_{\text{in}}(\beta, \sigma; V) = \frac{P(\beta, \sigma)}{\sqrt{1 + 2\kappa V^2}} \equiv P(\beta, \sigma) \cos \theta, \quad (14)$$

where P is given by equation (12). That is, $|\theta| > 0$ decreases the power of the input beam relative to its unperturbed value (i.e. relative to the power of the exact solution with the same parameters). Figure 4(a) suggests that there is a minimum power P_{min} that can sustain a propagating soliton; when $P_{\text{in}} < P_{\text{min}}$, one expects that no stationary states exist and that the input beam will transform into radiation modes [30]. Thus, $(\beta_{\text{min}}, P_{\text{min}})$ are the coordinates of the local minimum in the $P(\beta)$ curve (see figure 6(a)). One can then expect to encounter a maximum perturbation, against which the soliton is stable, through the following condition: $P_{\text{in}} = P_{\text{min}}$ when $|\theta| = |\theta|_{\text{max}}$. It can then be shown that for any input beam with $\beta > \beta_{\text{min}}$,

$$\tan (|\theta|_{\text{max}}) = \left[\left(\frac{P}{P_{\text{min}}} \right)^2 - 1 \right]^{1/2}. \quad (15)$$

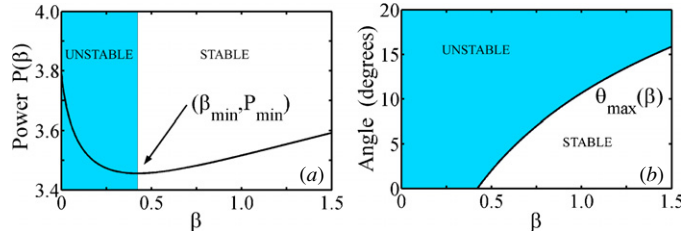


Figure 6. (a) Beam power calculated from equation (12) for hyperbolic soliton (3) with $\sigma = 1.4$, where $(\beta_{\min}, P_{\min}) \simeq (0.42, 3.46)$. The criterion $dP/d\beta > 0$ is met when $\beta > \beta_{\min}$ (unshaded region). (b) Theoretical prediction from equation (15) for the maximum launching angle of input beam (13) before the onset of instability, where $P_{\text{in}} \leq P_{\min}$.

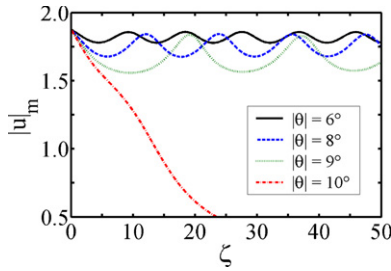


Figure 7. Long-lived self-persistent reshaping oscillations in the peak amplitude $|u|_m$ of a perturbed (conditionally stable) hyperbolic soliton (3) with $\sigma = 1.4$. For $\beta = 1$, equation (15) predicts that $|\theta|_{\max} \simeq 10.7^\circ$. Instability sets in when $|\theta|$ is slightly less than the theoretical value of $|\theta|_{\max}$.

Equation (15) assumes that the energy of the input and asymptotic beams are identical, and that radiation shed during reshaping can be neglected. Regions of predicted stability are illustrated in figure 6(b) for $\sigma = 1.4$. The simulations shown in figure 7 are in good agreement with equation (15), though instability sets in when $|\theta|$ is slightly less than the theoretical $|\theta|_{\max}$. This difference indicates that, as might be expected, stronger radiation shedding can come into play when the perturbed soliton approaches the instability threshold (the fraction of energy transferred to radiation modes will depend upon system parameters). Below the instability threshold (i.e. $|\theta| < |\theta|_{\max}$ so that $P_{\text{in}} > P_{\min}$), perturbed solitons undergo long-lived self-sustained oscillations in their parameters; we classify such solitons as stable limit-cycle attractors [36, 38]. These quasi-periodic orbits are effectively internal modes, and they have been analysed by Pelinovsky *et al* [30]. As the threshold is approached (i.e. $|\theta| \rightarrow |\theta|_{\max}$, or $P_{\text{in}} \rightarrow P_{\min}$), one finds that the evolving soliton diffracts towards a zero-amplitude state (see figure 7).

4.3. Algebraic solitons

Analysing the stability of algebraic solitons is a notoriously difficult task. Conventional nonlinear-perturbative techniques tend to become frustrated in all but the simplest cases because of their relatively slow asymptotics (i.e. power-law instead of exponential) [30]. Some insight can be gained from inspection of figure 4(a). For example, in the region where the hyperbolic solutions are unconditionally stable ($0 < \sigma \leq 1$), the beam power has a positive slope (i.e. $dP/d\beta > 0$) at $\beta = 0$. However, when $\sigma > 1$, one finds that $dP/d\beta < 0$ at $\beta = 0$. Thus, algebraic solitons are expected to be always unstable when $\sigma > 1$. Micallef *et al* [17] suggested that paraxial algebraic solitons (11b) are inherently unstable due to the absence

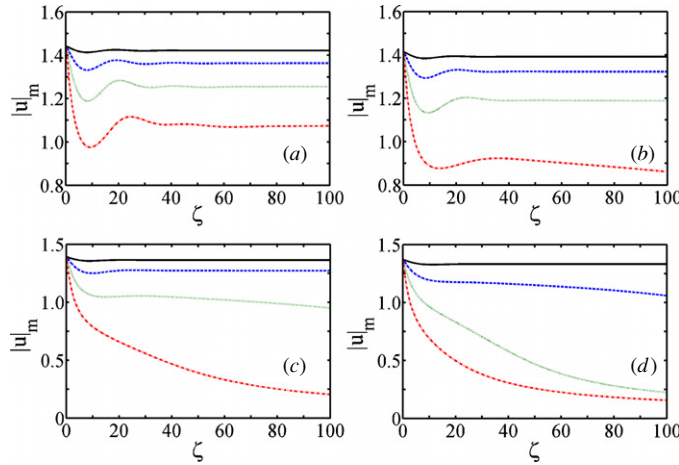


Figure 8. Evolution of the peak amplitude $|u|_m$ of a perturbed algebraic bright soliton when (a) $\sigma = 0.5$, (b) $\sigma = 0.6$, (c) $\sigma = 0.7$ and (d) $\sigma = 0.8$. Solid lines: $|\theta| = 10^\circ$; dashed lines: $|\theta| = 20^\circ$; dotted lines: $|\theta| = 30^\circ$; dot-dashed lines: $|\theta| = 40^\circ$.

of an arbitrary internal parameter. Their simulations confirmed that, even when $0 < \sigma \leq 1$, algebraic solitons are weakly unstable. Pelinovsky *et al* attributed this instability to resonant interactions with infinitely long linear waves [30].

We now undertake a fully nonlinear (i.e. numerical) stability analysis of Helmholtz algebraic solitons through consideration of the input beam:

$$u(\xi, 0) = \eta_a (a^2 \xi^2 + 1)^{-1/\sigma} \exp\left(-i \frac{V}{\sqrt{1 + 2\kappa V^2}} \xi\right). \quad (16)$$

The initial condition (16) corresponds to launching solution (4) without the beam-broadening factor $(1 + 2\kappa V^2)^{1/2}$. Analysis predicts that when $P_{in} < P$ (i.e. $|\theta| > 0$), any perturbed algebraic soliton with $0 < \sigma < 4$ will transform into radiation modes [30]. However, our simulations have shown that when σ is sufficiently less than 1, this collapse may be suppressed. The reshaping properties of algebraic solitons can thus be reminiscent of those of their hyperbolic counterparts. Figure 8 shows that as $\sigma \rightarrow 1$, the stability of algebraic solitons gradually diminishes. For instance, the solution in media characterized by $\sigma = 0.5$ is robust against all four increasingly strong angular perturbations (see figure 8(a)); the solution with $\sigma = 0.8$ is robust only against the weakest perturbation (see figure 8(d)).

5. Helmholtz algebraic dark solitons

5.1. Exact analytical solutions

Equation (2) permits the existence of algebraic dark solitons in the particular case of a cubic-quintic nonlinearity (i.e. when $\sigma = 2$). In symmetric form,

$$u(\xi, \zeta) = v \left(\xi \cos \theta + \frac{\zeta}{\sqrt{2\kappa}} \sin \theta \right) \left[a^2 \left(\xi \cos \theta + \frac{\zeta}{\sqrt{2\kappa}} \sin \theta \right)^2 + 1 \right]^{-1/2} \\ \times \exp \left[i \sqrt{\frac{1 + 4\kappa\mu}{2\kappa}} \left(-\xi \sin \theta + \frac{\zeta}{\sqrt{2\kappa}} \cos \theta \right) \right] \exp \left(-i \frac{\zeta}{2\kappa} \right), \quad (17)$$

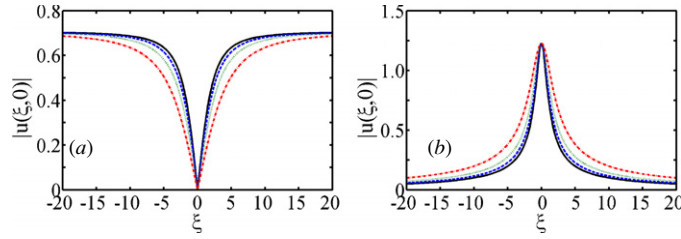


Figure 9. Comparison of the angular beam broadening effect for the algebraic dark soliton (17) (a) with that of the corresponding (i.e. $\sigma = 2$) bright soliton (4) (b). As $\xi \rightarrow \pm\infty$, one finds that the dark solution behaves as $u \sim \pm v/a$ (reflecting the π phase shift). Solid line (black): $\theta = 0^\circ$ (the paraxial profile); dashed line (blue): $|\theta| = 30^\circ$; dotted line (green): $|\theta| = 45^\circ$; dot-dashed line (red): $|\theta| = 60^\circ$. Other parameters: $\alpha = \gamma = 1$.

where $a^2 \equiv \alpha^2/6\gamma$, $v \equiv (3/\alpha)^{1/2}a^2$ and $\mu \equiv -\alpha^2/4\gamma$. Like its bright counterpart (solution (4)), the dark solution is specified uniquely by the choice of α and γ . There is a phase shift of π radians across the transverse extent of the field, and an absolute zero in the field at the beam centre (see figure 9). However, the solution is structurally distinct from the more familiar phase-topological dark solitons [40, 41]. In passing, we note an asymmetry between algebraic solutions (17) and (4) (in the case of $\sigma = 2$)—while the intensity profiles of canonical bright and black Kerr solitons, $I_b = \text{sech}^2(s)$ and $I_d = \tanh^2(s)$, are related by $I_d = 1 - I_b$, the same type of relationship does not hold for bright and dark algebraic beams.

One can now consider the multiple limit $\kappa \rightarrow 0$, $\kappa\mu \rightarrow 0$ and $\kappa V^2 \rightarrow 0$. From the forward solution, one can recover the paraxial soliton of Hayata and Koshiba [13], namely

$$u(\xi, \zeta) \sim v(\xi + V\zeta)[a^2(\xi + V\zeta)^2 + 1]^{-1/2} \exp\left[-iV\xi + i\left(\mu - \frac{V^2}{2}\right)\zeta\right]. \quad (18a)$$

The backward solution tends to

$$u(\xi, \zeta) \sim v(\xi + V\zeta)[a^2(\xi + V\zeta)^2 + 1]^{-1/2} \exp\left[iV\xi - i\left(\mu - \frac{V^2}{2}\right)\zeta\right] \exp\left(-i2\frac{\zeta}{2\kappa}\right), \quad (18b)$$

which has no counterpart in paraxial theory due to the rapid-phase κ -dependent term that survives the limit. It is interesting to note that equation (2) supports both bright and dark algebraic solitons without needing to reverse the relative signs of the nonlinear terms.

5.2. Numerical stability analysis

The apparent absence of a suitable stability criterion has so far rendered an in-depth analysis of solution (17) problematic. For instance, one cannot apply the renormalized-momentum integral [42] since there is no intrinsic-velocity parameter [41]. One also encounters divergences in the integral conserved quantities (equations (8a)–(8c)) because the solution does not break up in the way the renormalization method demands (i.e. a plane-wave background modulated by an obliquely propagating grey ‘dip’).

Here, we investigate the stability properties of Helmholtz algebraic dark solitons numerically using the input beam

$$u(\xi, 0) = v\xi(a^2\xi^2 + 1)^{-1/2} \exp\left(-iV\sqrt{\frac{1 + 4\kappa\beta}{1 + 2\kappa V^2}}\xi\right). \quad (19)$$

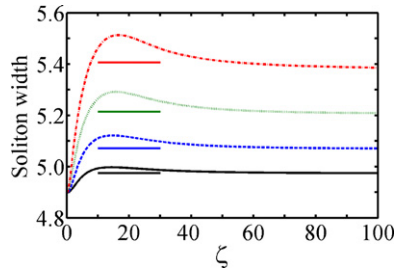


Figure 10. Evolution of the beam full-width of a perturbed algebraic dark soliton. The width tends asymptotically towards the value $\Lambda_\infty \sim (1+2\kappa V^2)^{1/2}\Lambda_0$, where $\Lambda_0 \equiv 2/a$ (horizontal bars). Solid line (black): $|\theta| = 10^\circ$; dashed line (blue): $|\theta| = 15^\circ$; dotted line (green): $|\theta| = 20^\circ$; dot-dashed line (red): $|\theta| = 25^\circ$. The widths have been calculated by fitting the numerical data to the nonlinear refractive-index function $n_{NL} = -\alpha|u|^2 + \gamma|u|^4$ in combination with solution (17). For larger values of $|\theta|$, the evolving beam radiates more strongly and suffers fluctuations to its shape that can complicate interpolation. Other parameters: $\alpha = \gamma = 1$.

This initial condition corresponds to launching an exact paraxial soliton (that does not account for the beam-broadening factor). The full width of the beam is found to tend towards an asymptotic value $\Lambda_\infty = (2/a)(1+2\kappa V^2)^{1/2}$ as $\zeta \rightarrow \infty$, eventually leaving a stationary beam (see figure 10). Simulations show that the dark beam can be robust against perturbations, even though its bright counterpart (solution (4) with $\sigma = 2$) is always unstable. Thus, one can interpret the dark solitons as fixed-point attractors. Similar qualitative behaviour has been uncovered in the propagation properties of Helmholtz Kerr dark solitons [41].

6. Conclusions

We have presented a variety of new exact analytical solutions to a generalized cubic-quintic nonlinear Helmholtz equation, including hyperbolic and algebraic solitons, and transversely periodic waves. The mathematical origin of the bright algebraic family lies in taking a particular limit of the hyperbolic family. We have shown that a fully self-consistent transition from a hyperbolic soliton into an algebraic soliton can be achieved using the Helmholtz formalism. New conservation laws have been reported. The conserved quantities have been evaluated exactly for algebraic solitons, and a classical particle energy–momentum relationship has been uncovered for Helmholtz solitons. Well-known paraxial results [13, 17] have also emerged from a quite general limit process. The stability of Helmholtz bright solitons has been investigated by combining conventional semi-analytical techniques [30, 37] with beam geometry in the (x, z) frame [35, 39], and simulations have generally supported our predictions. In particular, new regimes (within $0 < \sigma < 1$) have been uncovered in which algebraic solitons demonstrate stable-attractor properties when subject to large angular perturbations. Numerical analysis has also provided evidence of algebraic dark-soliton stability.

The new solitons reported here have innate mathematical appeal as exact solutions to generic non-integrable elliptic equations. Our results are also of physical interest, particularly in photonics, where we propose that Helmholtz soliton theory will play a central role in the design of future integrated-optic devices that exploit non-trivial angular geometries. Indeed, the coexistence of many different solution families (plane waves, hyperbolic and algebraic solitons) could open up the possibility of exciting new multiplexing [21] and interface [22] applications within Helmholtz-nonparaxial configurations.

References

- [1] Dodd R K, Eilbeck J C, Gibbon J D and Morris H C 1982 *Solitons and Nonlinear Wave Equations* (London: Academic)
Remoissenet M 1999 *Waves Called Solitons: Concepts and Experiments* 3rd edn (Berlin: Springer)
Infeld E and Rowlands G 2000 *Nonlinear Waves, Solitons and Chaos* 2nd edn (Cambridge: Cambridge University Press)
- [2] Kivshar Y S and Malomed B A 1989 *Rev. Mod. Phys.* **61** 763
- [3] Klaus M, Pelinovsky D E and Rothos V M 2006 *J. Nonlinear Sci.* **16** 1
Ablowitz M J and Satsuma J 1977 *J. Math. Phys.* **19** 2180
- [4] Pelinovsky D E and Grimshaw R H J 1997 *Phys. Lett. A* **229** 165
Ono H 1976 *J. Phys. Soc. Japan* **41** 1817
- [5] Brunhuber C, Mertens F G and Gaididei Y 2007 *Eur. Phys. J B* **57** 57
- [6] Fokas A S, Pelinovsky D E and Sulem C 2001 *Physica D* **152** 189
Satsuma J and Ablowitz M J 1979 *J. Math. Phys.* **20** 1496
Watanabe Y and Tajiri M 1998 *J. Math. Phys.* **67** 705
Tajiri M, Arai T and Watanabe Y 1998 *J. Phys. Soc. Japan* **67** 4051
- [7] Pelinovsky D E and Sulem C 1998 *J. Math. Phys.* **39** 6551
Benjamin T B 1966 *J. Fluid Mech.* **25** 241
Ono H 1975 *J. Phys. Soc. Japan* **39** 1082
Meiss J D and Pereira N R 1978 *Phys. Fluids* **21** 700
- [8] Kennel C F, Buti B, Hada T and Pellat R 1988 *Phys. Fluids* **31** 1949
- [9] Manakov S V, Zakharov V E, Bordag L A, Its A R and Matveev V B 1977 *Phys. Lett. A* **63** 205
- [10] Skryabin D V and Yulin A V 2006 *Phys. Rev. E* **74** 046616
- [11] Belenov E M and Poluéktov I A 1969 *Sov. Phys.—JETP* **28** 754
Hanamura E 1974 *J. Phys. Soc. Japan* **37** 1598
- [12] Mihalache D, Truta N, Panoiu N C and Baboiu D M 1993 *Phys. Rev. A* **47** 3190
Mihalache D and Panoiu N C 1993 *J. Phys. A: Math. Gen.* **26** 2679
- [13] Hayata K and Koshiba M 1995 *Phys. Rev. E* **51** 1499
Hayata K and Koshiba M 1995 *Opt. Lett.* **20** 1131
- [14] Hayata K and Koshiba M 1994 *J. Opt. Soc. Am. B* **11** 2581
Hayata K and Koshiba M 1995 *Phys. Rev. E* **51** 5155
- [15] Alatas H, Iskandar A A, Tjia M O and Valkering T P 2006 *Phys. Rev. E* **73** 066606
Grimshaw R and Malomed B 1994 *Phys. Rev. Lett.* **72** 949
- [16] 't Hooft G 1976 *Phys. Rev. Lett.* **37** 8
Polyakov A M 1974 *JETP Lett.* **20** 194
- [17] Micallef R W, Afansjev V V, Kivshar Y S and Love J D 1996 *Phys. Rev. E* **54** 2936
- [18] Kivshar Y S 1998 *Opt. Quantum Electron.* **30** 571
Kivshar Y S and Luther-Davies B 1998 *Phys. Rep.* **298** 81
Stegeman G and Segev M 1999 *Science* **286** 1518
- [19] Zakharov V E and Shabat A B 1972 *Sov. Phys.—JETP* **34** 62
Satsuma J and Yajima N 1974 *Suppl. Prog. Theor. Phys.* **55** 284
Gordon J P 1983 *Opt. Lett.* **8** 596
Cohen O, Uzdin R, Carmon T, Fleischer J W, Segev M and Odouov S 2002 *Phys. Rev. Lett.* **89** 133901
- [20] Aceves A B, Moloney J V and Newell A C 1989 *Phys. Rev. A* **39** 1809
Aceves A B, Moloney J V and Newell A C 1989 *Phys. Rev. A* **39** 1828
- [21] Chamorro-Posada P and McDonald G S 2006 *Phys. Rev. E* **74** 036609
- [22] Sánchez-Curto J, Chamorro-Posada P and McDonald G S 2007 *Opt. Lett.* **32** 1126
- [23] Feit M D and Fleck J A 1988 *J. Opt. Soc. Am. B* **5** 633
- [24] Chamorro-Posada P, McDonald G S and New G H C 2002 *J. Opt. Soc. Am. B* **19** 1216
Laine T A and Friberg A T 2000 *J. Opt. Soc. Am. B* **17** 751
Blair S 2000 *Chaos* **10** 570
Sheppard A P and Haelterman M 1998 *Opt. Lett.* **23** 1820
Fibich G 1996 *Phys. Rev. Lett.* **76** 4356
- [25] Lax M, Louisell W H and McKnight W B 1975 *Phys. Rev. A* **11** 1365
- [26] Chi S and Guo Q 1995 *Opt. Lett.* **20** 1598
- [27] Ciattoni A, Crosignani B, Di Porto P, Scheuer J and Yariv A 2006 *Opt. Express* **14** 5517
Ciattoni A, Crosignani B, Mookherjea S and Yariv A 2005 *Opt. Lett.* **30** 516

- Crosignani B, Yariv A and Mookherjea S 2004 *Opt. Lett.* **29** 1524
Ciattoni A, Di Porto P, Crosignani B and Yariv A 2000 *J. Opt. Soc. Am. B* **17** 809
- [28] Mihalache D, Bertolotti M and Sibilica C 1989 *Progress in Optics* 27 ed E Wolf (Amsterdam: Elsevier) p 229
Snyder A W and Mitchell D J 1993 *Opt. Lett.* **18** 101
- [29] Pushkarov K I, Pushkarov D I and Tomov I V 1979 *Opt. Quantum Electron.* **11** 471
Pushkarov K I and Pushkarov D I 1980 *Rep. Math. Phys.* **17** 37
- [30] Pelinovsky D E, Afanasjev V V and Kivshar Y 1996 *Phys. Rev. E* **53** 1940
- [31] Akhmediev N, Ankiewicz A and Grimshaw R 1999 *Phys. Rev. E* **59** 6088
- [32] Biswas A 2004 *Opt. Commun.* **235** 183
- [33] Goldstein H 1982 *Classical Mechanics* 2nd edn (Reading, MA: Addison-Wesley)
- [34] Chamorro-Posada P, McDonald G S and New G H C 2001 *Opt. Commun.* **192** 1
- [35] Chamorro-Posada P, McDonald G S and New G H C 1998 *J. Mod. Opt.* **45** 1111
- [36] Christian J M, McDonald G S and Chamorro-Posada P 2007 *J. Phys. A: Math. Theor.* **40** 1545
Christian J M, McDonald G S and Chamorro-Posada P 2007 *J. Phys. A: Math. Theor.* **40** 8601 (corrigendum)
- [37] Vakhitov M G and Kolokolov A A 1973 *Radiophys. Quantum Electron.* **16** 783
Laedke E W, Spatschek K H and Stenflo L 1983 *J. Math. Phys.* **24** 2764
- [38] Christian J M, McDonald G S and Chamorro-Posada P 2007 *Phys. Rev. A* **76** 033833
Christian J M, McDonald G S and Chamorro-Posada P 2007 *Phys. Rev. A* **76** 033834
Christian J M, McDonald G S and Chamorro-Posada P 2007 *Phys. Rev. A* **76** 049905 (erratum)
- [39] Chamorro-Posada P, McDonald G S and New G H C 2000 *J. Mod. Opt.* **47** 1877
- [40] Zakharov V E and Shabat A B 1973 *Sov. Phys.—JETP* **37** 823
- [41] Chamorro-Posada P and McDonald G S 2003 *Opt. Lett.* **28** 825
- [42] Pelinovsky D E, Kivshar Y S and Afansjev V V 1996 *Phys. Rev. E* **54** 2015
Barashenkov I V 1996 *Phys. Rev. Lett.* **77** 1193
Kivshar Y S and Afansjev V V 1996 *Opt. Lett.* **21** 1135
Kivshar Y S and Królkowski W 1995 *Opt. Lett.* **20** 1527